

Superthermal Electron Processes in the Upper Atmosphere  
of Uranus: Aurora and Electroglow

J. H. Waite, Jr. and M. O. Chandler  
Space Science Laboratory  
NASA Marshall Space Flight Center  
Huntsville, Alabama 35812

R. V. Yelle and B. R. Sandel  
Lunar and Planetary Laboratory  
The University of Tucson  
Tucson, Arizona

87 MAY 11 A8:54

RECEIVED  
A.L.A.A.  
U.S. LIBRARY

Abstract

Strong ultraviolet emissions from the upper atmosphere of Uranus suggest that both auroral and electroglow phenomena are of significant aeronomical consequences in the structure of the upper atmosphere. Combined modeling and data analysis have been carried out to determine the effect of electroglow and auroral phenomena on the global heat and atomic hydrogen budgets in the Uranus upper atmosphere. The results indicate that the auroral and electroglow heat sources are not adequate to explain the high exospheric temperature observed at Uranus, but that the atomic hydrogen supplied by these processes is more than sufficient to explain the observations. The various superthermal electron distributions modeled have significantly different efficiencies for the various processes such as UV emission, heating, ionization, and atomic hydrogen production and produce quite different H<sub>2</sub> band spectra. However, additional information on the UV spectra and global parameters is needed before modeling can be used to distinguish between the possible mechanisms for electroglow.

## I. INTRODUCTION

International Ultraviolet Explorer observations by Clarke [1982] and Durrance and Moos [1982] of H Ly  $\alpha$  at Uranus indicated unexpectedly large planetary emissions and were the first suggestion that particle-induced excitation was important in the Uranus system. Voyager Ultraviolet Spectrometer (UVS) measurements verified the existence of particle-induced H Ly  $\alpha$  emissions at Uranus and suggested that both "electroglow" processes and auroral particle precipitation processes were important sources of ultraviolet emissions [Broadfoot et al., 1986].

Uranus is the third outer planet to show indications of a UV emission phenomenon curiously confined to the sunlit portion of the planet and recently termed "electroglow" [Broadfoot et al., 1986]. The existence of unexpectedly bright H<sub>2</sub> band emissions suggests that superthermal electrons are responsible for the phenomenon yet there does not appear to be sufficient energy available from photoelectrons to reproduce the observed emission intensities [Chandler et al., 1986]. Recent analysis of limb scan profiles at Saturn [Yelle et al., 1986] and at Uranus [Broadfoot et al., 1986] suggests that the emission intensities peak relatively deep in the atmosphere near an H<sub>2</sub> density of  $10^{11}$  to  $10^{13}$  cm<sup>-3</sup>. A corresponding emission peak in the Ly  $\alpha$  limb scan profile further suggests that optically thin, Doppler-shifted Ly  $\alpha$  emissions may also be associated with the electroglow process. The limb scan data have prompted Clarke [1986] to suggest an atmospheric dynamo as the mechanism for

energization of electrons. Spectral differences are observed in the UVS spectra for electroglow emissions at Jupiter, Saturn, and Uranus which are explained by Shemansky [1986] as the consequences of changes in the energy of the exciting electrons.

On the other hand auroral emissions at Uranus have been observed on both the dayside and nightside at Uranus and appear to be reasonably well ordered by the highly eccentric magnetic field of Uranus [Sandel, 1986]. The spectral characteristics of the emissions show a clear dominance of H<sub>2</sub> Lyman and Werner band emissions similar to auroral emissions at Saturn and are suggestive of energetic electrons (~10 keV) incident on an H<sub>2</sub> atmosphere.

The major objectives of this paper are to use the constraints of the Voyager UVS data set with regard to atmospheric structure, magnetic location, and intensity and spectral content of the observed UV emissions in conjunction with a model atmosphere to point out the aeronomical consequences of the particles which may produce these emissions. We include energetic electron precipitation for the auroral case and several different possible superthermal electron populations for electroglow.

## II. THE MODEL

The calculations presented here are derived from a comprehensive one-dimensional model of the upper atmospheres of the outer planets used previously to study the aeronomical effects of superthermal electron processes at Saturn [Waite,

1981], at Jupiter [Waite et al., 1983], and at Uranus [Chandler and Waite, 1986].

The model includes solutions to the coupled continuity, momentum, and energy equations for the major neutral and ion species. It also provides a complete description of the energy loss and transport of superthermal electrons in the upper atmosphere using a two-stream electron transport code. This allows us to study the aeronomical processes associated with photoelectron and auroral electrons including atomic hydrogen production, ion production, excitation of UV emissions, and heating of the neutral and electron gases.

The neutral atmosphere is the same as used in Chandler and Waite [1986] with a new temperature profile derived from Voyager data. The temperatures were taken from results of the infrared interferometer spectrometer (IRIS), the radio science instrument (RSS), and the ultraviolet spectrometer (UVS). The values used are shown in Table 1. Linear interpolation was used between these data points.

Standard continuity and momentum (diffusion) equations are solved for all the major neutral species:  $H_2$ , He, H,  $CH_4$ ,  $C_2H_2$ ,  $C_2H_4$ , and  $C_2H_6$ . The lower boundary mixing ratios for  $CH_4$  and  $C_2H_2$  are inferred from the Voyager UVS measurements [Broadfoot et al., 1986]. The chemical reactions for the neutral atmosphere are basically the same as in Strobel [1969, 1975], although with updated reaction rates and cross sections [Yung and Strobel, 1980; Atreya et al., 1981]. A diffusion equation for  $H^+$  is also solved, and photochemical solutions are obtained for the

following short-lived ions:  $C_2H_5^+$ ,  $CH_5^+$ ,  $CH_4^+$ ,  $CH_3^+$ ,  $CH_2^+$ ,  $CH^+$ ,  $He^+$ ,  $HeH^+$ ,  $H_2^+$ , and  $H_3^+$ . The chemical reactions listed in Waite [1981] or Atreya and Donahue [1976] were used in the ionospheric calculations. The eddy diffusion coefficient is inferred from Voyager UVS measurements [Broadfoot et al., 1986]. The neutral and ionospheric components of the model are coupled with the superthermal electron transport code and run until a steady state solution is reached. A detailed description of all aspects of this model is given by Waite [1981].

#### Photoproduction and Electron Impact Cross Sections

$H_2$ , He, and H can be photoionized by radiation with wavelengths shorter than 804, 504, and 912 Å, respectively. References for photoabsorption, photoionization, and photodissociation can be found in Waite [1981] or Atreya et al. [1981]. However, the solar flux is extremely weak at Uranus thereby accentuating the relative importance of superthermal electron processes. In order to calculate electron impact ionization, airglow excitation, neutral atmospheric heating, dissociation, and ambient electron heating from superthermal electrons, it is necessary to determine the electron flux as a function of energy, altitude, and direction.

The two-stream method was used in our model for both the photoelectron and energetic electron flux calculations, and it is described in Nagy and Banks [1970] and Banks and Nagy [1970]. The pitch angle distribution of electrons is approximated by two streams of electrons, one going up and the other going down. We

used 0.5-eV wide bins below 10 eV, gradually increasing to 400 eV wide bins near 10 keV.

Elastic electron impact cross sections for He and H were taken from Moiseiwitsch [1962]. Inelastic cross sections for He and H were taken from Jackman et al. [1977] and Olivero et al. [1973]. The H<sub>2</sub> elastic cross section, the elastic backscatter probability, and the inelastic H<sub>2</sub> backscatter probability were derived from recent differential elastic cross section measurements of Shyn and Sharp [1980, 1981]. The backscatter probabilities for energies greater than 1 keV were extrapolated.

The different sets of inelastic electron impact cross sections reported in the literature are in reasonably good agreement with the exception of the excitation of the C<sup>1</sup> $\pi_u$  state (upper level of the Werner band system) [Miles et al., 1972; Cravens, 1974; Gerhart, 1975; Garvey et al., 1977; Ajello et al., 1984]. We used the Garvey et al. [1977] cross section set for our general energy loss cross sections, i.e., our calculations of electron fluxes. Yet for calculations of individual production rates such as Lyman and Werner band production, H<sub>2</sub> dissociation, dissociative excitation, vibrational excitation, rotational excitation, and H<sub>2</sub> ionization, we used the cross section set of [Ajello et al., 1984; D. E. Shemansky, private communications, 1987].

We calculate only the total integrated band intensities for the Lyman and Werner band systems; however, it should be pointed out that these total intensities could be broken down into individual band intensities in the manner described in Cravens

[1974] or [Yung et al., 1982]. Radiative transfer effects are also not considered for the Lyman and Werner bands; this confines us to accurate descriptions of these emissions above the hydrocarbon layer (180 km) and above the level of H<sub>2</sub> multiple scattering fluorescence effects at H<sub>2</sub> column depths exceeding 10<sup>20</sup> cm<sup>-3</sup> (600 km). We are, in most cases, justified in ignoring radiative transfer effects for the H<sub>2</sub> band systems, since the 20% enhancement of the Lyman bands due to Rayleigh scattering of H<sub>2</sub> [Yung et al., 1982] is within the present uncertainty of the cross sections. Radiative transfer effects cannot be ignored for Lyman alpha; the values are good to only a factor of 2.

Ultraviolet emissions represent only a small fraction of the total energy deposited in the atmosphere by superthermal electrons and EUV radiation. Energy can also be deposited as ionization, dissociation, vibrational excitation, neutral heat, and/or electron heat. The rate at which superthermal electrons heat the ambient electrons is given by Swartz et al. [1971]. The amount of neutral heat and dissociation that results directly from electron impact on H<sub>2</sub> can be calculated in the manner described by Cravens et al. [1975]. There are also indirect sources of heat from other processes taking place after the initial excitation of H<sub>2</sub> (or H or He). These will be discussed in the following section on the temperature structure.

### The Thermospheric Temperature Structure

Electron impact processes in an H<sub>2</sub>-dominated atmosphere lead to substantial heating of the neutral atmosphere as well as

production of atomic hydrogen and ultraviolet emissions. The relative efficiency for heating depends on the altitude and energy distribution of the superthermal electrons. Standard photoelectron heating processes have a heating efficiency of over 60%; whereas, precipitating electron beams have a heating efficiency of 30% to 55%, depending on the incident energy of the beam and the time history of precipitation [Waite et al., 1983]. The heating results from several processes.

Although the relative importance of the various processes is dependent on the details of the superthermal energy distribution general statements can be made as to their order of importance. The major heating process is chemical heating due to the formation of  $H_2^+$  and subsequent reactions which result in the recombination of  $H_3^+$  to produce  $H_2$  and  $H$ . The importance of this process therefore depends on the relative efficiency for the ionization of  $H_2$  which increases as the superthermal electron energy reaches 100 eV and is highly dependent on induced compositional changes in the atmosphere. The overall process releases 10.95 eV of heat per  $H_2$  ionization but can be short-circuited if  $H_2^+$  charge exchanges with  $H$  and the  $H^+$  formed in this reaction radiatively recombines. The second most important mechanism is electron impact dissociation of  $H_2$ . Dissociation of the  $b^3\Sigma$  state of  $H_2$  is by far the most important dissociation process liberating 5.5 eV per dissociation. Its importance is increased by the cascading from the  $a^3\Sigma$  and  $c^3\Pi$  states to the  $b^3\Sigma$  state. Dissociative excitation processes give 3.5 eV per dissociation. Thermal electron cooling of the superthermal

electrons and subsequent  $H_2$  vibrational and rotational cooling of the thermal electrons is the third most important source of heating. Another important electron impact heat source comes from vibrational excitation of the ground electronic state of  $H_2$  following Lyman and Werner band transitions. The  $B^1\Sigma$  and  $C^1\Pi$  excited states radiate to the  $H_2$  ground electronic state forming the Lyman and Werner band systems, respectively. Many of these transitions leave the electron in excited vibrational states of the ground electronic state. Theoretical calculations by Cravens [1974] show that an average of 3.2 eV of vibrational energy is generated per Lyman emission, and 2.3 eV per Werner emission. Heat is produced since the vibrational redistribution time constant is less than the radiative time constant.

Cooling of the upper atmosphere of Uranus is achieved by infrared emissions. However, unlike the case of Jupiter and Saturn where the abundances of  $CH_4$ ,  $C_2H_2$ , and  $C_2H_6$  are relatively high in the homosphere, the cold trap in the case of Uranus keeps the relative abundance of hydrocarbons quite low in the upper atmosphere [Broadfoot et al., 1986]. The result is that the bulk of the IR cooling comes from the weak quadrupole emissions of  $H_2$  and as a consequence occurs quite low in the atmosphere, taken in the present model to be at the 0.1 mbar pressure level (D. F. Strobel, private communications, 1987).

Little is known of the dynamics of the upper atmosphere of Uranus. Convective processes may play an important role in determining the neutral temperature structure of the upper atmosphere. However, until the dynamics is better understood,

conduction will be the sole means of transporting heat for the present model. A conduction equation of the form

$$\frac{d}{dz} \left[ - r_n \frac{dT_n}{dz} \right] = Q_n - L_n ,$$

where

$$r = H_2 \text{ conductivity} = A T_n^s$$

$$A = 252 \text{ erg cm}^{-1} \text{ s}^{-1} \text{ K}^{-1}$$

$$s = 0.751 \text{ [Hanley et al., 1970]}$$

$Q_n$  = heat sources

$L_n$  = heat sinks

is used to determine the neutral temperature profile. The heat sink is considered to be infinite at the lower boundary (0.1 mbar pressure level) and fixed at a temperature of 100 K. The heat source terms as described above are distributed in altitude and calculated from the two-stream electron transport code. The equation is integrated to determine the resulting model temperature profile.

## Neutral Atmospheric Composition

The dominant species in the Uranus upper atmosphere is molecular hydrogen,  $H_2$ . Helium has a fractional mixing ratio of 0.15 [Hanel et al., 1986]. Atomic hydrogen becomes increasingly important at higher altitudes because it is produced by solar EUV photons and particle precipitation processes in the upper atmosphere near an atmospheric density level of  $10^{11} \text{ cm}^{-3}$  and can only be chemically lost through three-body processes deep in the atmosphere at an atmospheric density level greater than  $1 \times 10^{13} \text{ cm}^{-3}$ . Thus the high-altitude source, the low-altitude chemical sink, and the large Fickian scale height for the relatively light H atom result in H becoming the dominant constituent above an atmospheric density level of  $\sim 10^6 \text{ cm}^{-3}$ . While hydrocarbon molecules exist in significant quantities in the upper atmosphere of Jupiter and of Saturn, the cold tropospheric temperatures and relatively small eddy diffusion coefficient at Uranus result in a relative dearth of hydrocarbons in the Uranus upper atmosphere. A mixing ratio of  $10^{-6}$  for  $CH_4$  and for  $10^{-7}$  for  $C_2H_2$  and a homopause level at the  $2 \times 10^{14} \text{ cm}^{-3}$  atmospheric density level (420 km) has been inferred from occultation measurements made by the Voyager UVS during the Uranus encounter [Broadfoot et al., 1986]. More recent work by Yelle et al. [1987] suggests much lower mixing ratios for these constituents. However, the values we have used result in such small quantities of these hydrocarbons that they are already of little consequence to this study. The Voyager UVS also inferred high exospheric temperatures 750 K near the  $2 \times 10^{10} \text{ cm}^{-3}$  atmospheric density

level. This results in a greatly extended atmosphere at Uranus with a density level of atomic hydrogen of  $10^7 \text{ cm}^{-3}$  over 3500 km above the 100 mbar pressure level. (Note that all altitudes are given with respect to the 100 mbar level at ~25,750 km radial distance.) The atmosphere inferred from the Voyager UVS measurements is shown in Figure 1 along with the model atmosphere that would be expected from solar EUV processes alone, yet utilizing the Voyager UVS inferred neutral temperature structure.

The relatively good agreement for  $\text{H}_2$  is not surprising since it is near diffusive equilibrium in the model and we have adopted the same neutral temperature structure. Likewise, the  $\text{CH}_4$  has been forced into agreement by adjusting the eddy diffusion coefficient. A value of  $100 \text{ cm}^2 \text{ s}^{-1}$  has been used to obtain the best fit. On the other hand the model calculation for atomic hydrogen requires a proper description of all the chemical production and loss processes in the model to obtain the proper profile. The present model contains source terms due to the dissociation of  $\text{H}_2$  by EUV photons and photoelectrons and from the ionization of  $\text{H}_2$  by EUV photons and photoelectrons, followed by ion-neutral chemistry that results in the formation of  $\text{H}_3^+$  which eventually recombines to form  $\text{H}_2$  and H. Due to the lack of significant hydrocarbon concentrations the only real loss of H comes from the three-body reaction  $\text{H} + \text{H} + \text{H}_2 \rightarrow 2 \text{H}_2$ . The atomic hydrogen profile can be used along with the neutral temperature profile and  $\text{H}_2$  band emission profiles obtained from the UVS measurements to provide important constraints on the nature and strength of these additional particle-induced

processes. The agreement between the standard EUV model atmosphere and the UVS inferred atomic hydrogen density at 1800 km shown in Figure 1 is surprisingly good, questioning the need for additional sources of H atoms from superthermal electron processes such as aurora or electroglow.

### III. ELECTROGLOW

The UV emissions associated with the electroglow in the Uranus atmosphere are suggestive of collisional processes involving low-energy (<100 eV) electrons [e.g., Broadfoot et al., 1986; Prange, 1986]. Suggestions for the source of such electrons include precipitation, in situ generation, or local energization. Four different superthermal electron models are considered: (1) a composite precipitation spectrum, (2) a straight solar EUV photoelectron model, (3) a solar EUV photoelectron model with an enhanced production at a specific energy that varies from 10 to 35 eV and follows the altitude dependence of the photoelectrons, and (4) a solar EUV photoelectron distribution that has been energized by various amounts ranging from 5 to 15 eV to simulate the energization of photoelectrons by parallel electric fields or wave-particle processes. These various models are not based on any measured electron fluxes, but are simply chosen to illustrate the possible superthermal electron processes that may result in electroglow at Uranus.

### Enhanced Photoelectron Production

It was found that good agreement between the observed ultraviolet limb scan profiles and the model profiles was obtained if the energetic electrons were distributed in altitude like the photoelectrons. That is, new electrons were introduced into the "photoelectron" transport equations at a single energy and distributed in altitude with the functional form of the photoelectron production rate. Such processes could arise as the result of a significant intensification of EUV emissions incident on the Uranus upper atmosphere. Several different energies were used for the electrons in the model, ranging from 10 to 35 eV.

Table 2 shows the partitioning of electron energy among the various processes. At low "electroglow" energies (<15 eV), the majority of the energy goes into heating of the neutral gas and the ambient electrons. The other major energy sink is the dissociation of  $H_2$ . At energies above 15 eV the partitioning changes as more electrons have energy above the  $H_2$  ionization threshold. Neutral heating decreases, as does the dissociation of  $H_2$ , as more than 20% of the energy goes to ionize  $H_2$ . The electron heating remains about the same while airglow processes receive about twice as much energy as before. Thus the most obvious aeronomical consequences of the increase in energy of the locally generated energetic electrons are reduced direct neutral heating and  $H_2$  dissociation, along with increased  $H_2$  ionization and UV emissions. Superthermal electrons at 15 and 30 eV were chosen as representative of the extreme cases and are used in the next section to explore the aeronomical consequences of this scenario.

## Energy Gain

In the second scenario, all photoelectrons were assumed to be energized by some process (e.g., wave-particle interactions or electric fields) and gained a fixed amount of energy, between 5 and 18 eV. The resulting superthermal electron spectrum is significantly different, depending on the amount of energy gained. For low energies (e.g., 5 eV) the change from the initial photoelectron spectrum to the "heated" spectrum involves a redistribution of electrons below 10 eV (see Figure 2). The flux still drops sharply above 10 eV but now the electrons which were below 5 eV are bunched up between 5 and 10 eV. As the magnitude of the energy gain moves above 10 eV, two effects are evident. First, there is a significant increase in the flux above 10 eV resulting in increased emissions. Second, there is an increase in the cascading and/or secondary production which results in more flux at energies below 5 eV than in the small energy gain cases. The net result of this increase is more heating of the neutral atmosphere. For energy gain above 15 eV, several additional effects are noticeable. This case energizes electrons above the ionization threshold for H<sub>2</sub>. This produces a significant increase in the production of secondary electrons with energies below 10 eV. These electrons are then "heated" up to >15 eV and go through the cycle again. The result is large heating rates and atomic hydrogen production rates. This case also produces an order of magnitude increase in the UV emissions from H<sub>2</sub> and results in a runaway effect in the model since there

is no mechanism included which allows for "saturation" of the heating process.

This "heating" process shows similar variations in the partitioning of energy as a function of electron energy as in the previous case. The major difference between the two cases is in the electron heating, with the electron-energy gain process yielding about a factor of 5 less heat. This case also provides about 50% more energy to ionize  $H_2$ . In terms of UV emissions, about the same percentage of energy goes to producing Ly  $\alpha$  as before with a somewhat higher percentage going to Lyman band emissions.

To illustrate this case an energy gain of 13.5 eV per inelastic collision was chosen. This translates into the heating rate profile shown in Figures 3a and 3b.

### Electron Precipitation

Although the confinement of electroglow processes to the sunlit portion of the planet makes it difficult to envision a corresponding magnetospheric process responsible for the electroglow, we have considered this possibility for the sake of completeness. The precipitating electron energy spectrum was chosen to match the peak brightness and altitude variation of the UVS  $H_2$  limb scan profile. The required precipitating electron energy spectrum is shown in Figure 4. The broad range of electron energies required is determined by the broad altitude range of the limb scan emission feature. The increasing electron flux as a function of decreasing electron energy that is needed

is a consequence of the energy flux required at the higher altitudes and the decreasing efficiency for excitation of H<sub>2</sub> band emissions for lower-energy electrons.

### Aeronomical Consequences of Superthermal Electron Spectra in Electroglow Processes

The three types of emission-inducing particles considered in our study (i.e., precipitating electrons, enhanced photoelectron production, and heated photoelectrons) are all capable of reproducing the observed electroglow emissions from the Voyager limb scan in contrast to the small H<sub>2</sub> band emissions of the standard photoelectron case (also shown). Each process, however, results in a different partitioning of energy among the various energy loss mechanisms (e.g., airglow, heating, H production) and, as a result, gives rise to significantly different "atmospheres." To illustrate this we have tuned each process, in the model, to give a good representation to the UVS limb scan observations of H<sub>2</sub> band emissions. Figure 5 shows UVS inferred H<sub>2</sub> band emission limb scan profiles and model limb scans for: (1) enhanced photoelectron production at 15 eV, (2) enhanced photoelectron production at 30-eV, (3) energized photoelectrons (13.5 eV per inelastic collision), (4) a composite precipitating electron spectrum, and (5) the standard EUV photoelectron case. While the shape of the layers differs slightly between the processes, the differences are not significant. Conversely the energy partitioning and thus the energy flux required to match the limb scan data for the different cases varies

substantially. The 15-eV enhanced photoelectron production requires an energy flux of  $0.13 \text{ erg cm}^{-2} \text{ s}^{-1}$ ;  $0.035 \text{ erg cm}^{-2} \text{ s}^{-1}$  for 30-eV enhanced photoelectron;  $0.028 \text{ erg cm}^{-2} \text{ s}^{-1}$  for heated photoelectrons; and  $0.028 \text{ erg cm}^{-2} \text{ s}^{-1}$  for the precipitating electrons. Furthermore, the spectral characteristics of the four cases are quite different as illustrated by the varying Lyman to Werner band ratios: (1) 15 eV enhanced photoelectron production: 13; (2) 30 eV enhanced photoelectron production: 1.9; (3) heated photoelectrons: 2.8; and (4) precipitating electrons: 0.9. Unfortunately, at Uranus the spectral data are complicated by solar reflectance and cannot be used to distinguish the energy spectrum of electrons responsible for the electroglow. Table 2 gives the column emission rates, the column production rates and the column heating rates for all the superthermal electron distributions considered. Large variations are seen in the  $\text{H}_2$  dissociation rates, neutral heating rates, and direct  $\text{H}^+$  production rates.

#### Electroglow Atomic Hydrogen Production

We have calculated the self-consistent atomic hydrogen profiles for the cases outlined above. The density-versus-altitude profiles are shown in Figure 6. For the precipitating electron beam 6% of the energy goes into the production of atomic hydrogen. In the case of the superthermal electrons this number is 24% and 14% for the 15- and 30-eV cases, respectively. For the energization of photoelectrons the efficiency is 20%.

Analysis of the UVS results provided an atomic hydrogen number density of  $6.9 \times 10^7 \text{ cm}^{-3}$  at a  $\text{H}_2$  density level of  $1.16 \times 10^{10} \text{ cm}^{-3}$ . For our model atmosphere this  $\text{H}_2$  level occurs at 1800 km above the 100 mbar level. This level does not vary for the various cases considered. The model H density, however, does vary considerably from case to case. For example, in the case of locally generated 15-eV electrons the H density at 1800 km is  $1.3 \times 10^9 \text{ cm}^{-3}$ . The composite precipitation spectrum resulted in the lowest H density of  $2.5 \times 10^8 \text{ cm}^{-3}$ . Thus in each case - precipitating electrons, accelerated electrons, or locally produced electrons - the efficiency for dissociating  $\text{H}_2$  was too high and resulted in an H density larger than observed. Conversely, in the standard case with only solar EUV considered, the H density at 1800 km was  $8.0 \times 10^7 \text{ cm}^{-3}$ , in reasonable agreement with observations.

### Electroglow Heating

The Voyager observations provided some information on the thermal structure of the Uranian upper atmosphere (e.g., Voyager Uranus Science issue, Vol., 1986). However, most of the structure exists below the homopause (taken at the  $10^{-3}$  mbar level which corresponds to 420 km in our model) with the UVS data providing the only information above this level. The analysis of the UVS data [Broadfoot et al., 1986] gave a temperature of  $750 \text{ K} \pm 100 \text{ K}$  near the  $10^{10} \text{ cm}^{-3}$  density level (or 3500 km above the 100 mbar level in the model). Using the thermal conduction model described earlier, we calculated neutral temperature profiles for

the various cases (Figure 7). The standard photoelectron case produces a temperature profile which falls below the UVS temperature at 3500 km by over 600 K. All other cases produce better matches to the UVS data with the 15-eV magic electron case providing the closest fit. However, in all cases there is insufficient heating to explain the UVS inferred temperature profile.

#### IV. AURORA

The Voyager UVS measurements of the aurora at Uranus indicate dayside emissions coming from a few degree wide ring located between 30° and 45° co-latitude and nightside emissions coming from a circular region at the polar cap with 20 degree diameter [Sandel, 1986]. The auroral zone therefore covers an area between 2% and 4 % of the planet's total surface area, depending on the width of the dayside ring which is not well known at this time. The Voyager UVS measured the surface brightness in the H<sub>2</sub> bands to be ~9 kR and the Lyman alpha brightness to be ~1.5 kR, a ratio suggestive of electron bombardment on a pure H<sub>2</sub> atmosphere [Broadfoot et al., 1986].

We have used the two-stream electron transport code to model the effects of auroral electron precipitation on the atmosphere of Uranus. Two cases of monoenergetic electron beams were considered to parametrically study the range of possible cases, one at 1 keV and one at 10 keV. It was found that it was necessary to introduce an energy flux of 0.9 erg cm<sup>-2</sup> s<sup>-1</sup> in order to produce an H<sub>2</sub> band brightness of 9 kR. The fractional

energy depositions for the 1- and 10-keV beams are shown in Table 3 along with the column production rates for the various processes. In both cases the table gives the results for the beam incident on a solar-EUV-produced atmosphere (i.e., the standard atmosphere) and for the steady-state, converged auroral atmosphere. Due to time-dependent and horizontal transport effects, reality will lie somewhere in between.

The 10-keV electron precipitation case shows little change in fractional energy deposition as a result of atmospheric compositional changes from the standard EUV atmosphere to the auroral atmosphere since the electrons penetrate to a depth in the atmosphere (805 km) where the  $H_2$  concentration dominates that of H and is little changed by the auroral energy deposition. On the other hand, the 1-keV auroral case shows a marked change in fractional energy deposition as the atmospheric H: $H_2$  ratio is increased at the altitude of the electron penetration by electron impact production of H. In the 1-keV case this change in composition leads to a corresponding change in the Ly  $\alpha$  to  $H_2$  band column production ratio from about 0.11 in the EUV atmosphere to 0.36 in the auroral atmosphere. Indeed the efficiency of  $H_2$  band production is decreased enough in the auroral atmosphere that almost twice the energy flux of electrons would be needed to produce the observed UV emissions. The Ly  $\alpha$  to Lyman band ratio in the 10-keV case remains virtually the same as the atmosphere changes from EUV to auroral: 0.10 and 0.13. In fact the converged auroral atmosphere values are very close to those measured by the Voyager UVS and serve to quantify the claim

by Broadfoot et al. [1986] that the measured Ly  $\alpha$  to H<sub>2</sub> band emissions ratio is evidence for electron precipitation of electron with an energy of  $\sim 10$  keV.

The global auroral power suggested by these calculations lies somewhere between 1.7 and  $3.4 \times 10^{11}$  watts, depending on the fraction of the surface area affected by auroral processes. A large fraction of this energy goes into heating and production of atomic hydrogen. In the case of the 10-keV aurora,  $6.3 \times 10^{10}$  to  $1.3 \times 10^{11}$  watts of heat is dissipated in the upper atmosphere, and  $6.8 \times 10^{28}$  to  $1.4 \times 10^{29}$  H atoms per second are produced globally. For the 1-keV case the results are similar;  $5.8 \times 10^{10}$  to  $1.2 \times 10^{11}$  watts of heat and  $4.4 \times 10^{28}$  to  $8.8 \times 10^{28}$  H atoms per second are produced. The global effects of this heating and H production are illustrated in Figures 8 and 9 for the 10- and 1-keV aurora, respectively. The a plots show the altitude profiles of atomic hydrogen for the auroral atmosphere as well as cases where the auroral H production has been uniformly spread over the planet, assuming an auroral surface area of 2% and 4%. Similarly the b plots show the heat conduction calculations for the two auroral cases, assuming all heat is retained locally and for a situation where the heat has been uniformly spread over the planet, assuming fractional areas of 2% and 4% for the auroral zone.

The temperature profiles for the various cases suggest that local electron heating processes can marginally maintain a hot exosphere, but when spread over the planet the effect on the temperature structure is expected to be quite small. The

limitations of such calculations should not be overlooked, however. There is still quite a bit of uncertainty in the IR cooling process and in the time-dependent auroral energy input and morphology. Furthermore, the way we have uniformly spread the heat and the atomic hydrogen does not take into account the vertical motions of the atmosphere which must occur in the real dynamical expansion. However, the suggestion from the calculations is clear that auroral processes do indeed affect the atomic hydrogen budget significantly, yet they produce an insignificant amount of global heating.

## V. DISCUSSION

The observed UV emissions from the Uranus upper atmosphere have been taken as evidence for particle-induced excitation of  $H_2$ . This is based on our experience with auroral processes on the other planets. The results of our study provide constraints for the electroglow mechanism with regard to partitioning of the energy input. While electrons, produced from a variety of sources, are capable of giving good representations of the observed  $H_2$  band emissions, they give rise to aeromical effects which are not self-consistent with other observations of the upper atmosphere. In all of the cases considered here the efficiency for dissociating  $H_2$  was comparable to or significantly larger than the efficiency for producing  $H_2$  band emissions. On the other hand, as our standard model suggests, little, if any, additional atomic H production is occurring in the Uranus atmosphere. There does appear to be some additional heating

taking place since all of the sources of heating considered above were inadequate to produce the Voyager UVS inferred temperature profile. This conflicting aeronomical information may indeed provide important constraints on the superthermal electron distribution which arises from the electroglow mechanism.

The auroral models offer some additional interesting information on the temperature and atomic hydrogen budgets. As shown in Figures 8 and 9, by spreading the neutral heating and atomic hydrogen production over the entire planet we obtain results similar to those inferred from the electroglow modeling study. Particularly in the case of the 10-keV aurora, the globally averaged atomic hydrogen density at the 1800-km level is a factor of 2 higher than observed, while the global exospheric temperature should be affected very little.

Therefore, from the study of superthermal electron excitation of electroglow and precipitating electron excitation of aurora, the results are similar. More atomic hydrogen must be lost (or less produced) and additional sources of heating are required to explain the UVS data if they are indeed representative of global conditions at Uranus. The loss of atomic hydrogen may be facilitated by nonthermal processes [Broadfoot et al., 1987] and transport to the nightside. In the case of heating an additional heat source is required. Two possible suggestions include: (1) photoelectron heating from  $H^-$  ions upon absorption of long wavelength photons [Yelle et al., 1987], or (2) joule heating. As we have shown the various superthermal electron scenarios produce quite different  $H_2$  band

emission spectra, thus good spectral information on the H<sub>2</sub> band structure is needed before additional constraints can be put on the energy spectrum (and the mechanism for energization) of the superthermal electron processes which appear to be involved in the electroglow process.

### Electrical mechanisms

Several mechanisms have been suggested for the generation of electroglow. They include: (1) field-aligned acceleration of photoelectrons as a result of an atmospheric dynamo [Clarke, 1986], (2) precipitation of magnetospheric electrons (Curtis, private communication, 1987), (3) wave-particle energization of photoelectrons by ionospheric or magnetospheric plasma waves, (4) solar resonance scattering of Lyman and Werner band emission [Yelle et al., 1987], and (5) H<sub>3</sub><sup>+</sup> recombination with superthermal electrons [Yelle et al., 1987]. Furthermore, recent evidence presented by Yelle et al. [1987] suggests that the electroglow emission intensity at Jupiter, Saturn, and Uranus scales as the inverse square of the heliocentric distance independent of the solar cycle. If correct, this puts an interesting constraint on the electroglow process, since most photoelectron processes are controlled by photons below 2000 Å, a region of the solar flux that varies significantly through the course of the solar cycle. In light of current observational constraints let us examine the various mechanisms.

The atmospheric dynamo depends on the global thermospheric wind system of which little or nothing is known at the outer

planets. Although UV heating in the hydrocarbon layer is no doubt an important driver of the wind system that may well scale by the heliocentric distance, other thermospheric energy sources such as auroral processes are almost certainly important at Jupiter and joule heating may be significant at Uranus. These processes would not be expected to scale by the heliocentric distance. Furthermore, magnetic fields and ionospheric conductivities are quite different at Jupiter, Saturn, and Uranus and would significantly affect the strength of the atmospheric dynamo at these planets. Further calculations particularly of thermospheric wind systems are needed before this mechanism can be adequately evaluated. Our calculations do however demonstrate that energization of photoelectrons via atmospheric dynamo will produce the observed UV emissions. They do however require anomalous resistive properties which affect only the superthermal electrons or the joule heating of thermal electrons will be unexplainably large.

Precipitation of charged particles from the magnetosphere can produce the required UV emissions and in the case of Uranus a predominantly weaker magnetic field on the dayside of the planet will enhance dayside emission (Curtis, private communications, 1987). Such arguments will not however work at Jupiter or Saturn to produce the required day night asymmetry. Furthermore, electroglow emission intensities that scale as the inverse of the square of the heliocentric distance would not appear to be easily explained by this model. Nonetheless, Figure 5 shows the electron precipitation spectrum required to produce the Voyager

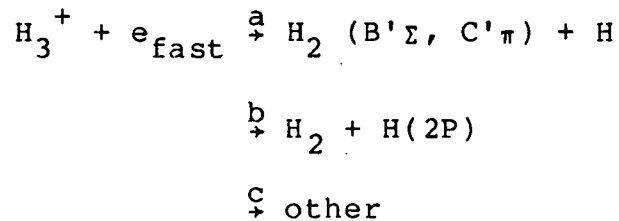
UVS electroglow limb scan. Voyager particle data must be examined to identify possible electron features in the magnetosphere.

Wave-particle energization of photoelectrons can reproduce the emissions. Again here as in the case of dynamo energization phase speeds of the waves must resonate with the superthermal and not the thermal electrons or tremendous power input (strong heating) will be required to produce a suitable emission intensity. The ionosphere or magnetosphere may be a source of the waves. One possibility is lower hybrid waves generated as a result of relative electron and ion drifts in the rapidly rotating planetary ionospheres in the outer planets. This particular mechanism needs examining further. Yet here again it is not clear why the mechanism would lead to the observed heliocentric scaling unless the electrons that are being accelerated are due to metallic ion formation from elements such as Na which appear to form sharp layers in the lower ionospheres of the outer planets.

Solar resonance scattering of the H<sub>2</sub> Lyman and Wesner bands is a source of emission that Yelle et al. [1987] have recently suggested has been underestimated in previous calculations. The limitations of this mechanism are that it would not appear to be able to reproduce the heliocentric variation for two reasons: (1) the scattering properties of the H<sub>2</sub> above the hydrocarbon absorption layer are quite different at Jupiter, Saturn, and Uranus, and (2) the region of the solar flux resonantly scattered in this mechanism is expected to vary by almost a factor of 2

over the solar cycle. Furthermore, it is not clear that this emission will have the appearance of "optically thin" emission as appears to be suggested by the Voyager UVS limb scan data.

A new mechanism concerning  $H_3^+$  recombination with fast electrons has been suggested by Yelle et al. [198]. The importance of this mechanism has not been carefully evaluated, but hinges around the branching ratio for the following processes which are not well known (H. H. Michels, private communications, 1987:



We can however estimate the strength of this mechanism making the following assumptions: (1) the photoelectron flux from 1 to 10 eV given by the model is  $\sim 10^5 \text{ cm}^{-2} \text{ s}^{-1} \text{ eV}^{-1}$ , (2) the cross section for the reaction is  $10^{-16} \text{ cm}^2$ , (3) the branching ratio is 1 ( $a = 1$ ) for  $H_2$  band emission, (4) the  $H_3^+$  density is  $10^4 \text{ cm}^{-3}$ , and (5) the scale height of the process is 1000 km as taken from the limb scan data. The resulting source strength is  $\sim 100 \text{ photons cm}^{-2} \text{ s}^{-1}$  which is 6 orders of magnitude too small to explain the observations. Yet clearly upper limits have been chosen in the calculation. A more exact calculation has been carried out using the model; the results are the same. The integrated column emission profile for  $H_2$  band emissions is 50 photons  $\text{cm}^{-2} \text{ s}^{-1}$  ( $5 \times 10^{-5} \text{ R}$ ). One way to increase the emission

is to enhance the low-energy (1-10 eV) superthermal electron flux. Yelle et al. [1987] have suggested that  $H^-$  formation and subsequent photodetachment in the near UV and visible can accomplish this. However, estimates made herein indicate that the average electron energy needed to initiate hydride formation via the process  $H_2^+ e_{fast} \rightarrow H^- + H$  is 3.5 eV and the average energy of the photoelectron resulting from photo-detachment is 2.5 eV. Therefore, the process is a net energy loss for the superthermal electrons, but an efficient way to dissociate  $H_2$ . Unfortunately, as our model calculations would indicate one needs to find ways to decrease not increase atomic hydrogen production in the electroglow mechanism.

No clear mechanism for electroglow production has yet emerged. Much additional work is needed to model the various suggested mechanisms. New high resolution spectra of the  $H_2$  band system would also be extremely helpful in determining the specifics of the superthermal electron distribution responsible for producing the observed emission. Further study of atomic hydrogen production and loss and upper atmospheric heating as a result of electroglow and auroral processes must be carried out before a self-consistent picture of the Uranus upper atmosphere can be produced.

## REFERENCES

- Ajello, J. M., D. Shemansky, T. L. Kwok, Y. L. Yung, Studies of extreme-ultraviolet emission from Rydberg series of  $H_2$  by electron impact, Phys. Rev. A., 29, 636, 1984.
- Atreya, S. K., and T. M. Donahue, Model ionospheres of Jupiter, in Jupiter, edited by T. Gehrels, pp. 304-318, University of Arizona Press, Tucson, 1976.
- Atreya, S. K., T. M. Donahue, and M. C. Festou, Jupiter: Structure and composition of the upper atmosphere, Astrophys. J. Lett., 247, L43, 1981.
- Banks, P. M., and A. F. Nagy, Concerning the influence of elastic scattering upon photoelectron transport and escape, J. Geophys. Res., 86, 8447, 1981.
- Broadfoot, A. L., et al., Ultraviolet spectrometer observations of Uranus, Science, 223, 74, 1986.
- Chandler, M. O., and J. H. Waite, Jr., The ionosphere of Uranus: A myriad of possibilities, Geophys. Res. Lett., 13, 6, 1986.
- Chandler, M. O., J. H. Waite, Jr., R. V. Yelle, and B. R. Sandel, Comparison of modeling results to the Voyager UVS Uranus observations, paper presented at Second Neil Brice Memorial Symposium, The University of Iowa, Iowa City, Iowa, September 1-5, 1986.

Clarke, J. T., Detection of auroral hydrogen Ly  $\alpha$  emission from Uranus, Astrophys. J. Lett., 263, L105, 1982.

Clarke, J. T., The post-Voyager significance of IUE observations of Uranus, paper presented at Second Neil Brice Memorial Symposium, The University of Iowa, Iowa City, Iowa, September 1-5, 1986.

Cravens, T. E., Astrophysical applications for electron energy deposition in molecular hydrogen, Ph.D. thesis, Harvard University, Cambridge, Mass., 1974.

Cravens, T. E., G. A. Victor, and A. Dalgarno, The absorption of energetic electrons by molecular hydrogen gas, Planet. Space Sci., 23, 1059, 1975.

Durrance, S. T., and H. W. Moos, Intense Ly  $\alpha$  emission from Uranus, Nature, 299, 428, 1982.

Garvey, R. H., H. S. Porter, and A.E.S. Green, Relativistic yield spectra for H<sub>2</sub>, J. Appl. Phys., 48, 4353, 1977.

Gerhart, D. E., Comprehensive optical and collision data for radiation action, 1, H<sub>2</sub>, J. Chem. Phys., 62, 821, 1975.

- Hanel, R., et al., Infrared observations of the Uranian System, Science, 233, 70, 1986.
- Jackman, C. H., R. H. Garvey, and A.E.S. Green, Electron impact on atmospheric gases, 1, Updated cross sections, J. Geophys. Res., 82, 5081, 1977.
- Miles, W. T., R. Thompson, and A.E.S. Green, Electron impact cross sections and energy deposition in molecular hydrogen, J. Appl. Phys., 43, 678, 1972.
- Moiseiwitsch, B. L., Elastic scattering of electrons, Atmos. Mol. Process., 280, 1981.
- Nagy, A. F., and P. M. Banks, Photoelectron fluxes in the ionosphere, J. Geophys. Res., 75, 6260, 1970.
- Olivero, J. J., J. N. Bass, and A.E.S. Green, Photoelectron excitation of the Jupiter dayglow, J. Geophys. Res., 78, 2812, 1973.
- Prange, R., New evidence for the role of photoelectrons in the H<sub>2</sub>-dayglow of the giant planets, Astron. Astrophys., 61, 11, 1986.

- Sandel, B. R., Coupling of the atmosphere and magnetosphere: UVS observations of Uranus, paper presented at Second Neil Brice Memorial Symposium, The University of Iowa, Iowa City, Iowa, September 1-5, 1986.
- Shemansky, D. E., The electroglow phenomenon: Jupiter, Saturn, and Uranus, paper presented at Second Neil Brice Memorial Symposium, The University of Iowa, Iowa City, Iowa, September 1-5, 1986.
- Shyn, T. W., and W. E. Sharp, Angular distribution of electrons elastically scattered from H<sub>2</sub>, Phys. Rev. A., 24, 1734, 1981.
- Strobel, D. F., The photochemistry of methane in the Jovian atmosphere, J. Atmos. Sci., 26, 906, 1969.
- Strobel, D. F., The photochemistry of hydrocarbons in the Jovian atmosphere, J. Atmos. Sci., 30, 489, 1973.
- Swartz, W. E., J. S. Nisbet, and A.E.S. Green, Analytic expression for the energy transfer rate from photoelectrons to thermal electrons, J. Geophys. Res., 76, 8425, 1971.
- Waite, J. H., Jr., The ionosphere of Saturn, Ph.D. dissertation, The University of Michigan, Ann Arbor, Michigan, 1981.

Waite, J. H., Jr., T. E. Cravens, J. U. Kozyra, A. F. Nagy, S. K. Atreya, and R. H. Chen, Electron precipitation and related aeronomy of the Jovian thermosphere and ionosphere, J. Geophys. Res., 88, 6143, 1983.

Yelle, R. V., B. R. Sandel, D. E. Shemansky, and S. Kumar, Altitude variation of EUV emissions and evidence for proton precipitation at low latitudes in the Saturnian atmosphere, J. Geophys. Res., 91, 8756, 1986.

Yelle, R. V., J. C. McConnell, B. R. Sandel, and A. L. Broadfoot, The dependence of electroglow on the solar flux, submitted to J. Geophys. Res., 1987.

Yung, Y. L., and D. F. Strobel, Hydrocarbon photochemistry and Lyman alpha albedo of Jupiter, Astrophys. J., 239, 395, 1980.

Yung, Y. L., G. R. Gladstone, K. M. Chang, J. M. Ajello, and S. K. Srivastava, H<sub>2</sub> fluorescence spectrum from 1200 to 1700 Å by electron impact: Laboratory study and application to Jovian aurora, Astrophys. J. Lett., 254, L65, 1982.

Table 1

Atmospheric Parameters

Pressure	Temperature	Atmospheric Number Density	Reference Altitude
100 mbar	52	$1.25 \times 10^{19}$	0
50 mbar	52	$6.28 \times 10^{18}$	15
20 mbar	56	$2.6 \times 10^{18}$	40
10 mbar	63	$1.2 \times 10^{18}$	55
1 mbar	88	$8.3 \times 10^{16}$	130
$10^{-3}$ mbar	130	$5.6 \times 10^{13}$	460
$2 \times 10^{-6}$ mbar	750	$2.0 \times 10^{10}$	1660

Table 2

## Efficiencies of Aeronautical Processes - Electrogrow

Case	Energy (eV)	Energy Input Rate ( $\text{eV S}^{-1}$ )	Column Emission Rates (R)			Heating Rates ( $\text{eV S}^{-1}$ )			Production Rates ( $\text{S}^{-1}$ )			
			Lyman $\alpha$	Lyman Bands	Werner Bands	Electron Gas Heating	Neutral Gas Heating	$\text{H}_2$ Dissociation	$\text{H}_2^+$ Production	$\text{H}^+$ Production	Dissociative $\text{H}^+$ Production	Direct $\text{H}^+$ Production
Local Creation	15	$1 \times 10^{11}$	264 (3%)	305 (3%)	22 (<1%)	$2.8 \times 10^{10}$ (37%)	$2.4 \times 10^{10}$ (30%)	$8.2 \times 10^9$ (24%)	$1.5 \times 10^7$ (<1%)	$2.0 \times 10^6$ (2%)	$9.3 \times 10^7$ (<1%)	
Local Creation	30	$2.5 \times 10^{10}$	77 (4%)	196 (8%)	105 (5%)	$4.6 \times 10^9$ (21%)	$4.4 \times 10^9$ (20%)	$1.3 \times 10^9$ (14%)	$3.1 \times 10^8$ (23%)	$4.5 \times 10^7$ (4%)	$2.4 \times 10^7$ (1%)	
Energy Gain	13	$1.4 \times 10^{10}$	42 (4%)	122 (11%)	44 (4%)	$2.4 \times 10^8$ (2%)	$2.5 \times 10^9$ (25%)	$9.2 \times 10^8$ (20%)	$1.8 \times 10^8$ (28%)	$1.4 \times 10^7$ (3%)	$5.7 \times 10^6$ (<1%)	
Precipitation	*		45 (3%)	134 (8%)	144 (9%)	$2.6 \times 10^9$ (17%)	$1.8 \times 10^9$ (11%)	$4.2 \times 10^8$ (6%)	$3.3 \times 10^8$ (34%)	$5.6 \times 10^7$ (7%)	$3.4 \times 10^7$ (3%)	

Table 3

## Efficiencies - Aurora

Case	Energy (eV)	Energy Input Rate (erg cm <sup>-2</sup> s <sup>-1</sup> )	Column Emission Rates (R)			Heating Rates (eV S <sup>-1</sup> )			Production Rates (s <sup>-1</sup> )			Direct H <sup>+</sup> Production
			Lyman α	Lyman Bands	Werner Bands	Electron Heating	Neutral Heating	Dissociative H <sub>2</sub>	H <sub>2</sub> <sup>+</sup> Production	H <sup>+</sup> Production		
Auroral Atmosphere	10K	0.9	1.2 x 10 <sup>3</sup> (3%)	4.3 x 10 <sup>3</sup> (9%)	4.9 x 10 <sup>3</sup> (11%)	2.7 x 10 <sup>10</sup> (6%)	5.9 x 10 <sup>10</sup> (13%)	1.2 x 10 <sup>10</sup> (6%)	1.1 x 10 <sup>10</sup> (41%)	2.0 x 10 <sup>9</sup> (9%)	8.3 x 10 <sup>8</sup> (2%)	
Non-Auroral Atmosphere	10K	0.9	1.0 x 10 <sup>3</sup> (2%)	4.5 x 10 <sup>3</sup> (9%)	5.2 x 10 <sup>3</sup> (11%)	7.9 x 10 <sup>9</sup> (2%)	7.9 x 10 <sup>10</sup> (17%)	1.3 x 10 <sup>10</sup> (6%)	1.2 x 10 <sup>10</sup> (43%)	2.1 x 10 <sup>9</sup> (9%)	1.4 x 10 <sup>7</sup> (<1%)	
Auroral Atmosphere	1K	0.9	2.0 x 10 <sup>3</sup> (5%)	2.6 x 10 <sup>3</sup> (6%)	3.0 x 10 <sup>3</sup> (7%)	9.2 x 10 <sup>10</sup> (22%)	2.5 x 10 <sup>10</sup> (6%)	6.0 x 10 <sup>9</sup> (3%)	7.0 x 10 <sup>9</sup> (27%)	1.2 x 10 <sup>9</sup> (6%)	5.1 x 10 <sup>9</sup> (17%)	
Non-Auroral Atmosphere	1K	0.9	1.1 x 10 <sup>3</sup> (3%)	4.5 x 10 <sup>3</sup> (9%)	5.1 x 10 <sup>3</sup> (11%)	1.8 x 10 <sup>10</sup> (4%)	6.8 x 10 <sup>10</sup> (15%)	1.4 x 10 <sup>10</sup> (7%)	1.2 x 10 <sup>10</sup> (42%)	2.0 x 10 <sup>9</sup> (9%)	1.3 x 10 <sup>8</sup> (<1%)	

## Figure Captions

Figure 1: Neutral atmosphere density and temperature profiles from the standard model along with densities inferred from the Voyager/UVS observations. The reference altitude is the 100 mbar pressure level.

Figure 2: Photoelectron flux spectra for the standard solar EUV case and heated photoelectron cases of 5 and 13.5 eV.

Figure 3: Heating rates for the "heated" photoelectron cases: a) as a function of photoelectron energy and b) the total rate versus altitude.

Figure 4: The flux spectrum of incident electrons used in the precipitation model of electroglow.

Figure 5: The resulting H<sub>2</sub> band emissions from the electroglow models converted to the Voyager limb scan geometry shown with the UVS observations.

Figure 6: Altitude profiles for atomic hydrogen from the electroglow models.

Figure 7: Resulting temperature profiles from the electroglow models along with the initial model temperature profiles inferred from Voyager data.

Figure 8: Altitude profiles for a) the atomic hydrogen and b) the temperature from the auroral model using 10 keV precipitating electrons.

Figure 9: Altitude profiles for a) the atomic hydrogen and b) the temperature from the auroral model using 1 keV precipitating electrons.

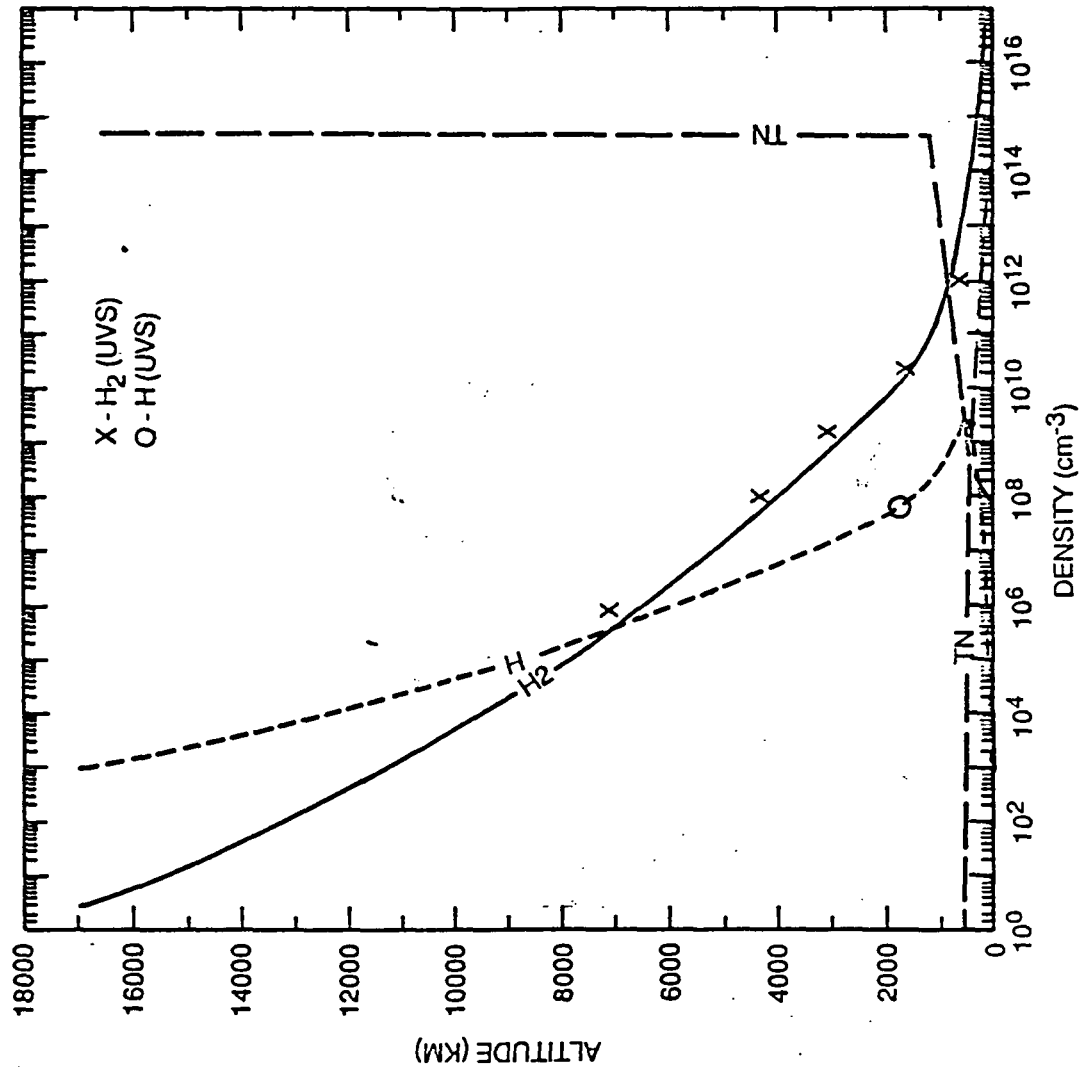


Figure 1

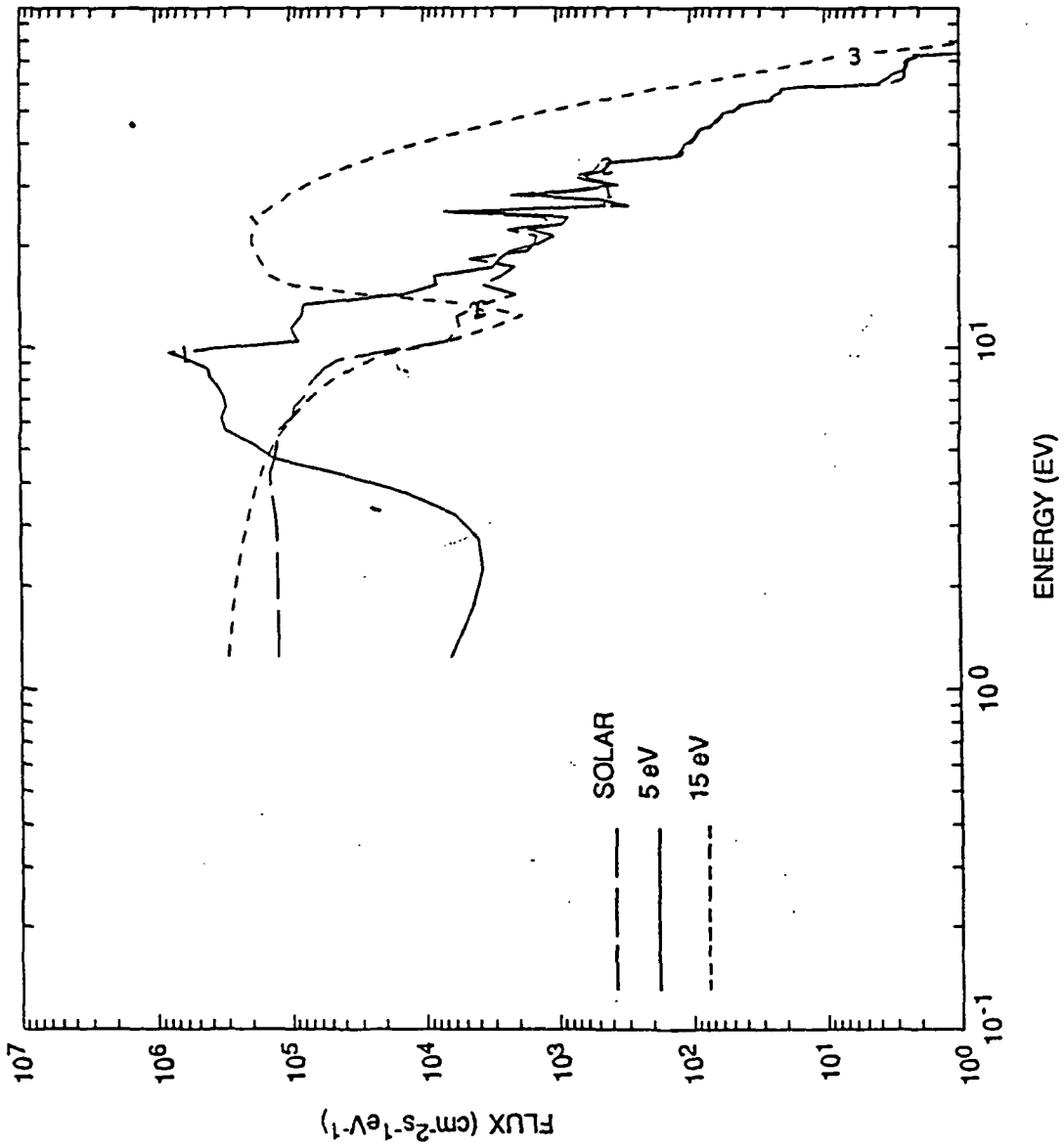


Figure 2

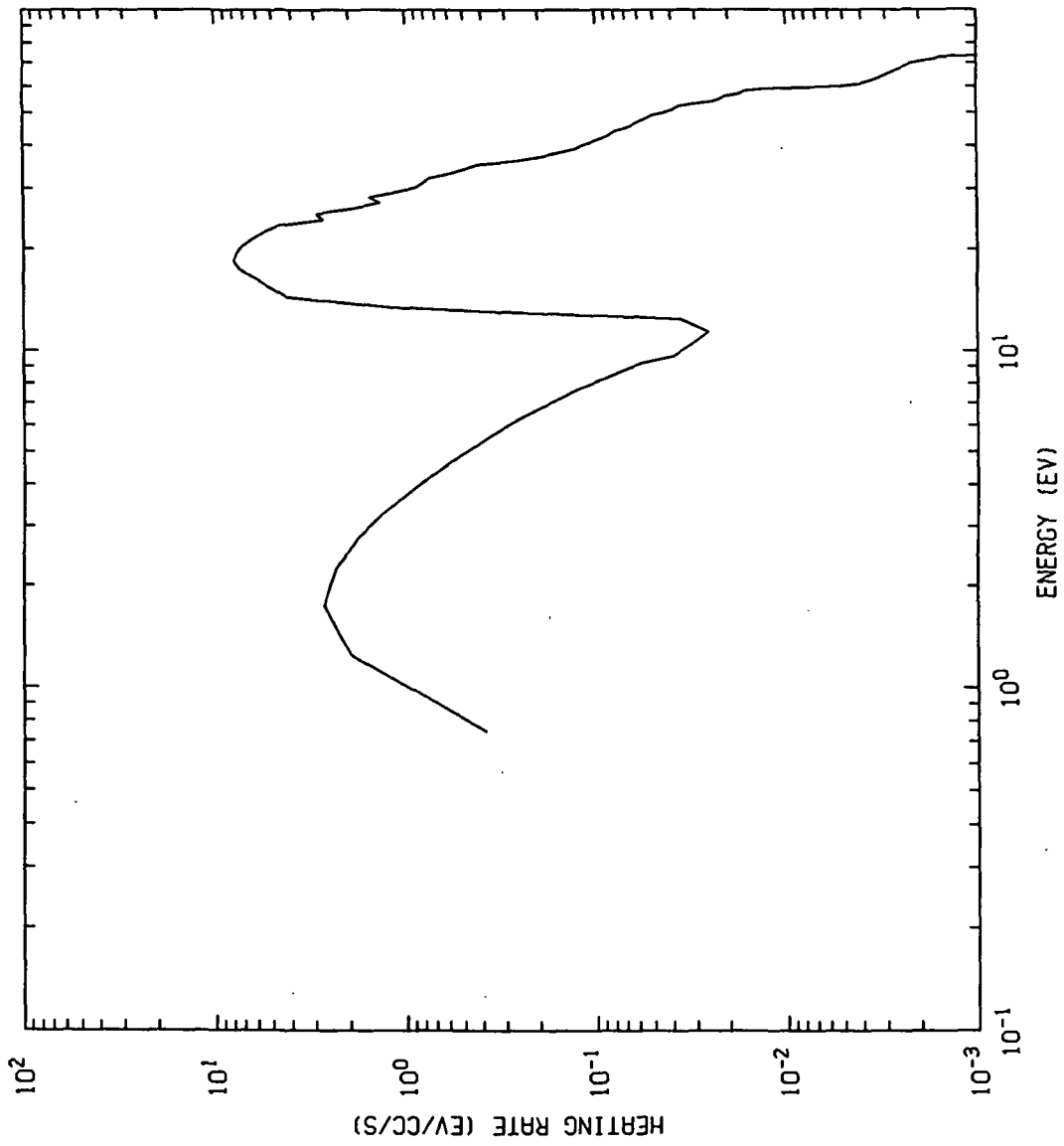


Figure 3a

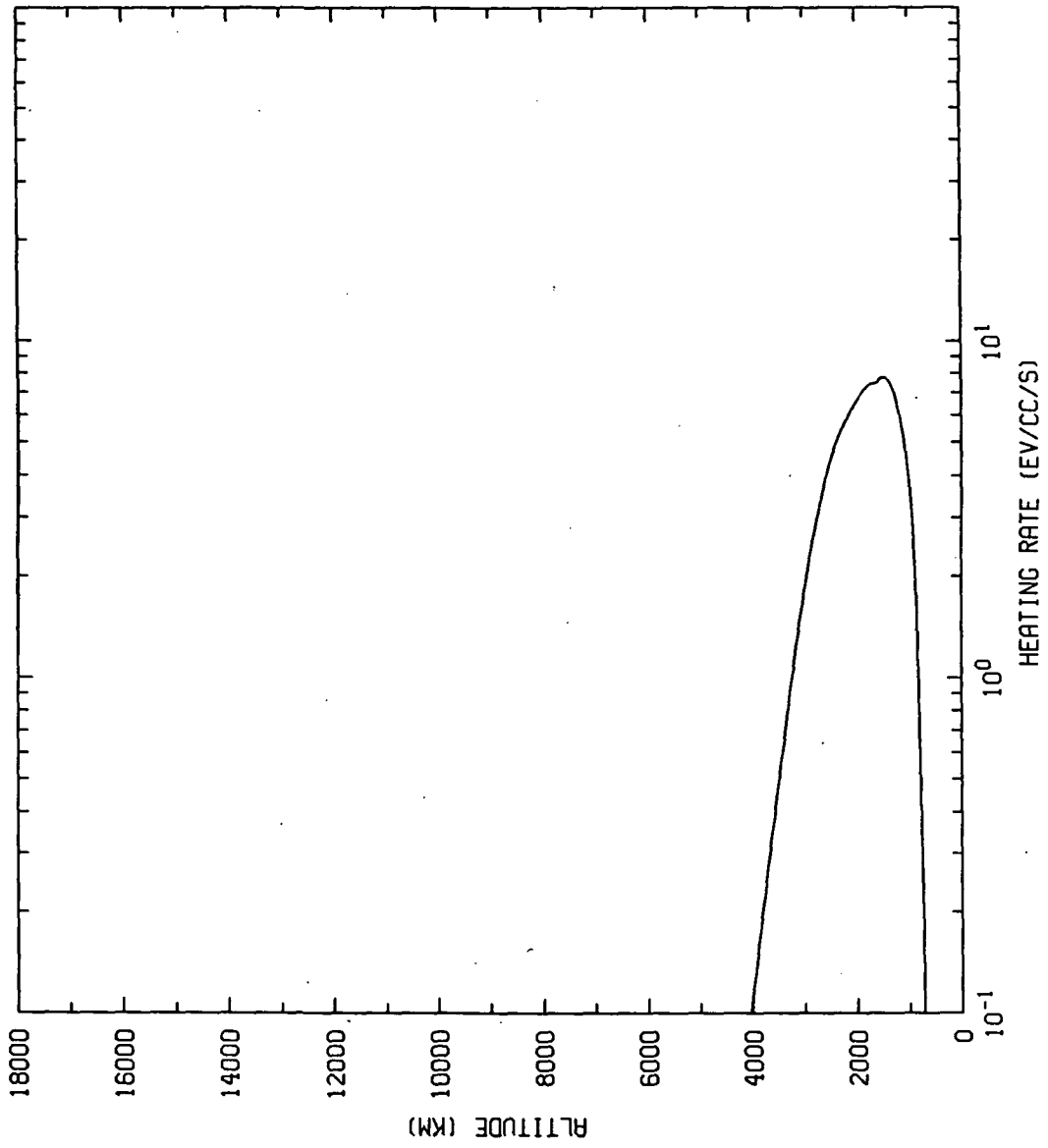


Figure 3b

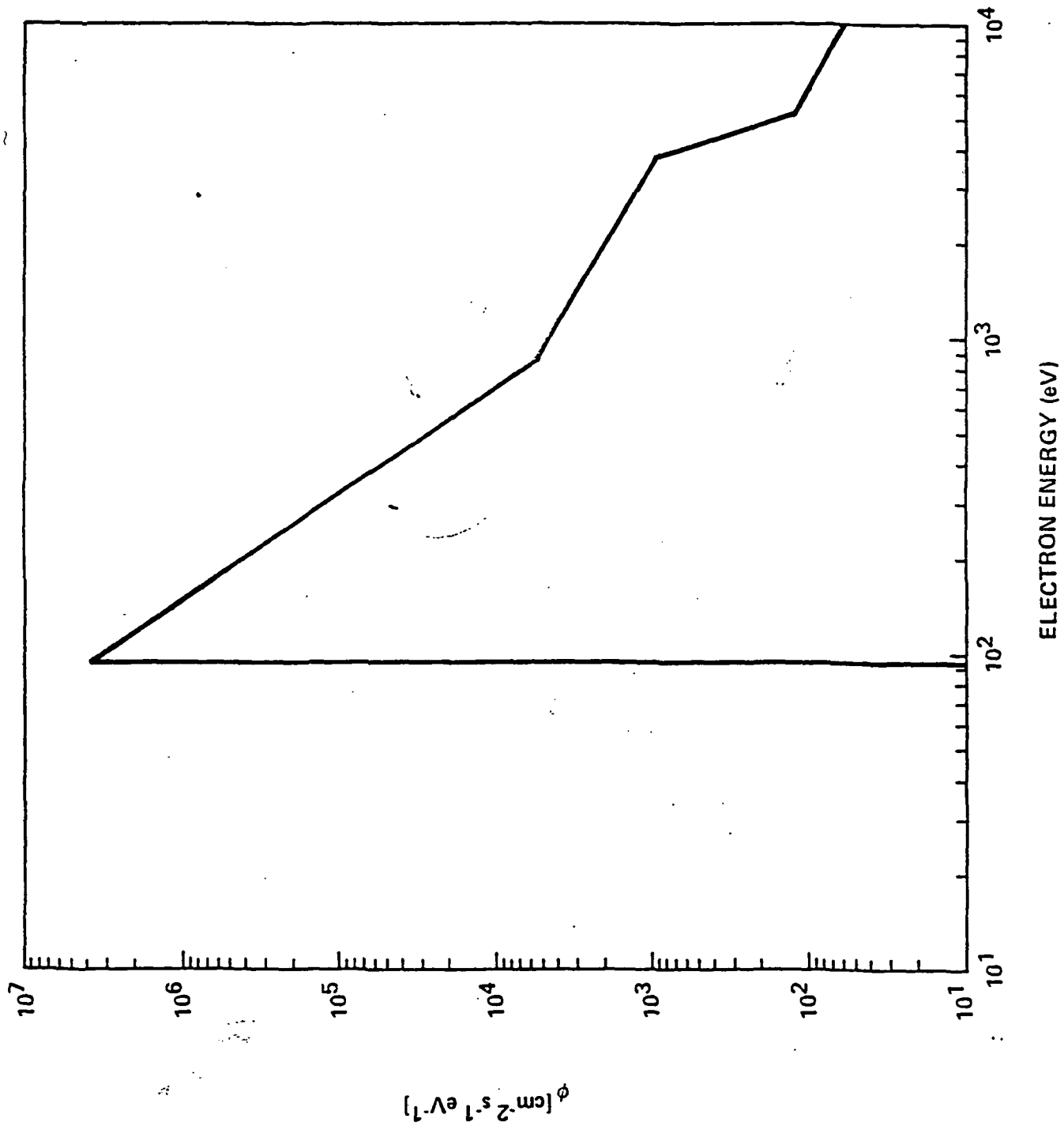


Figure 4

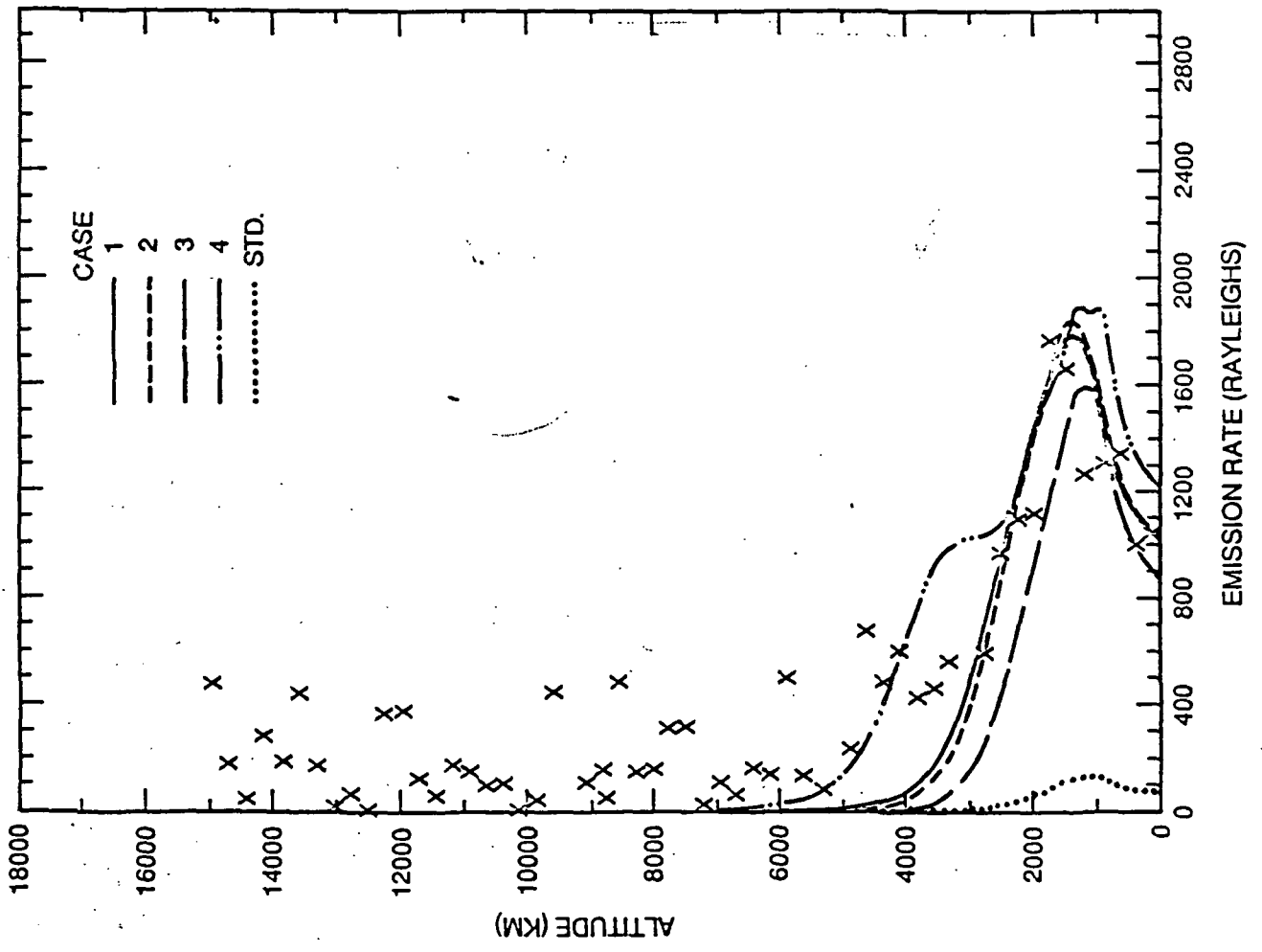


Figure 5

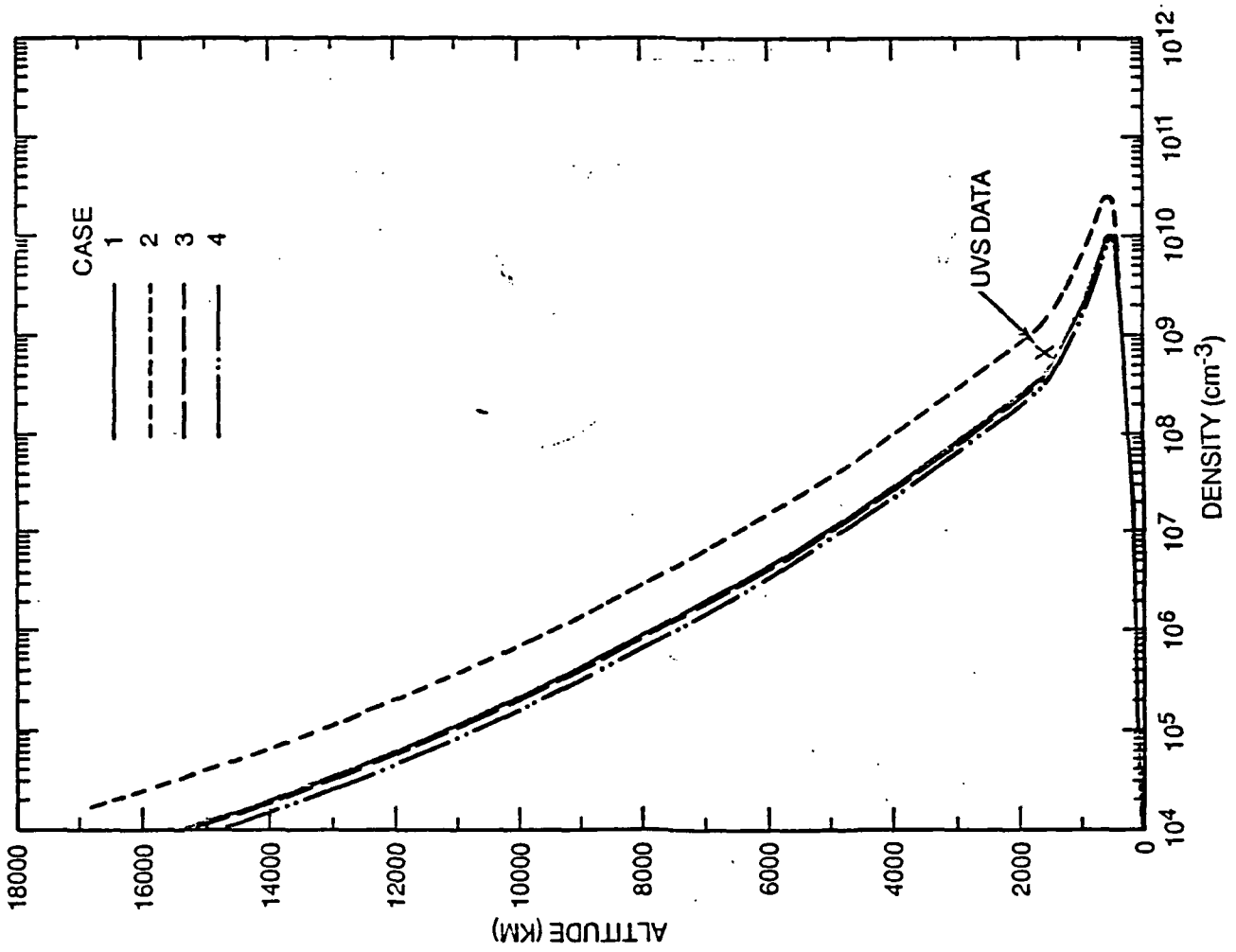


Figure 6

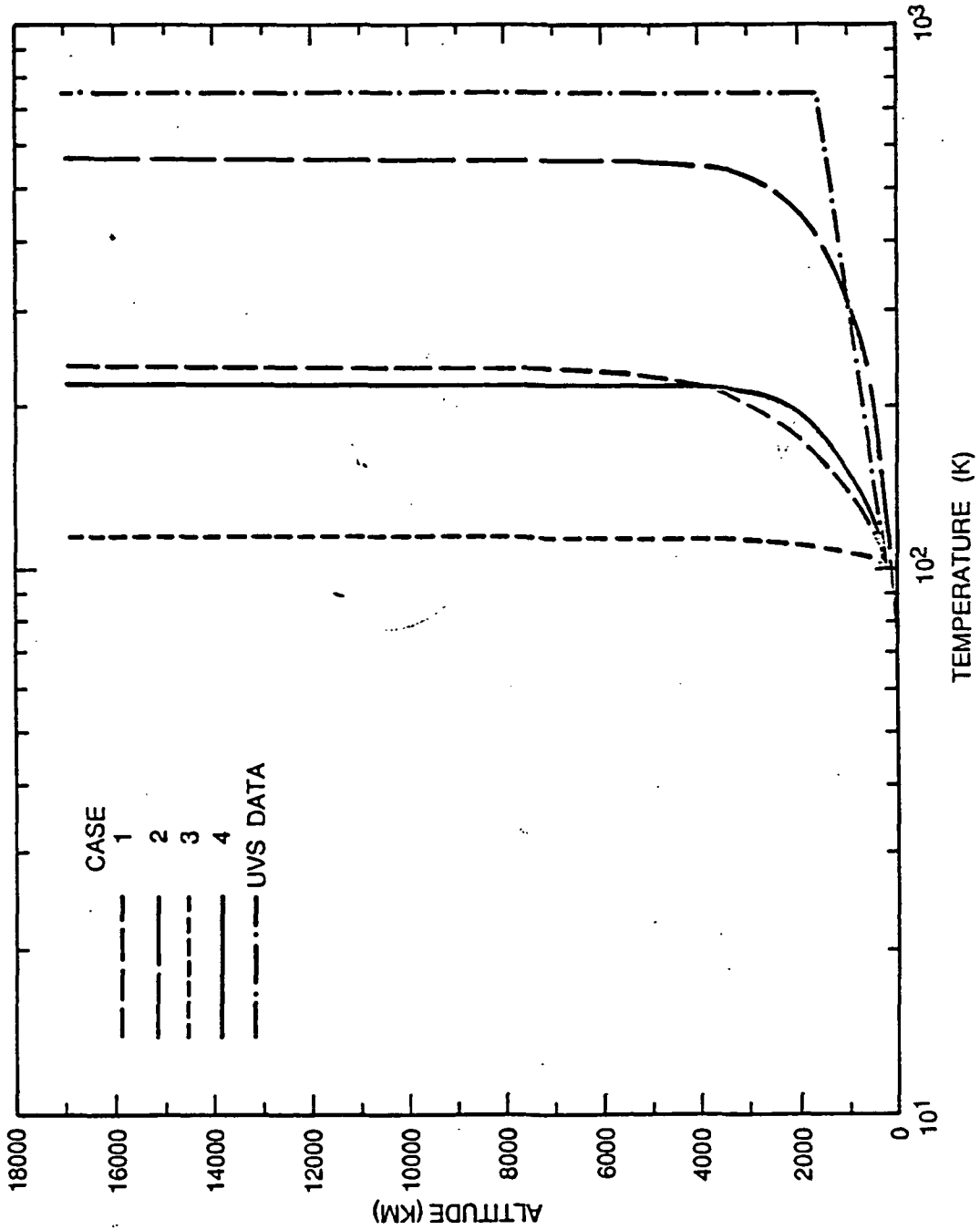


Figure 7

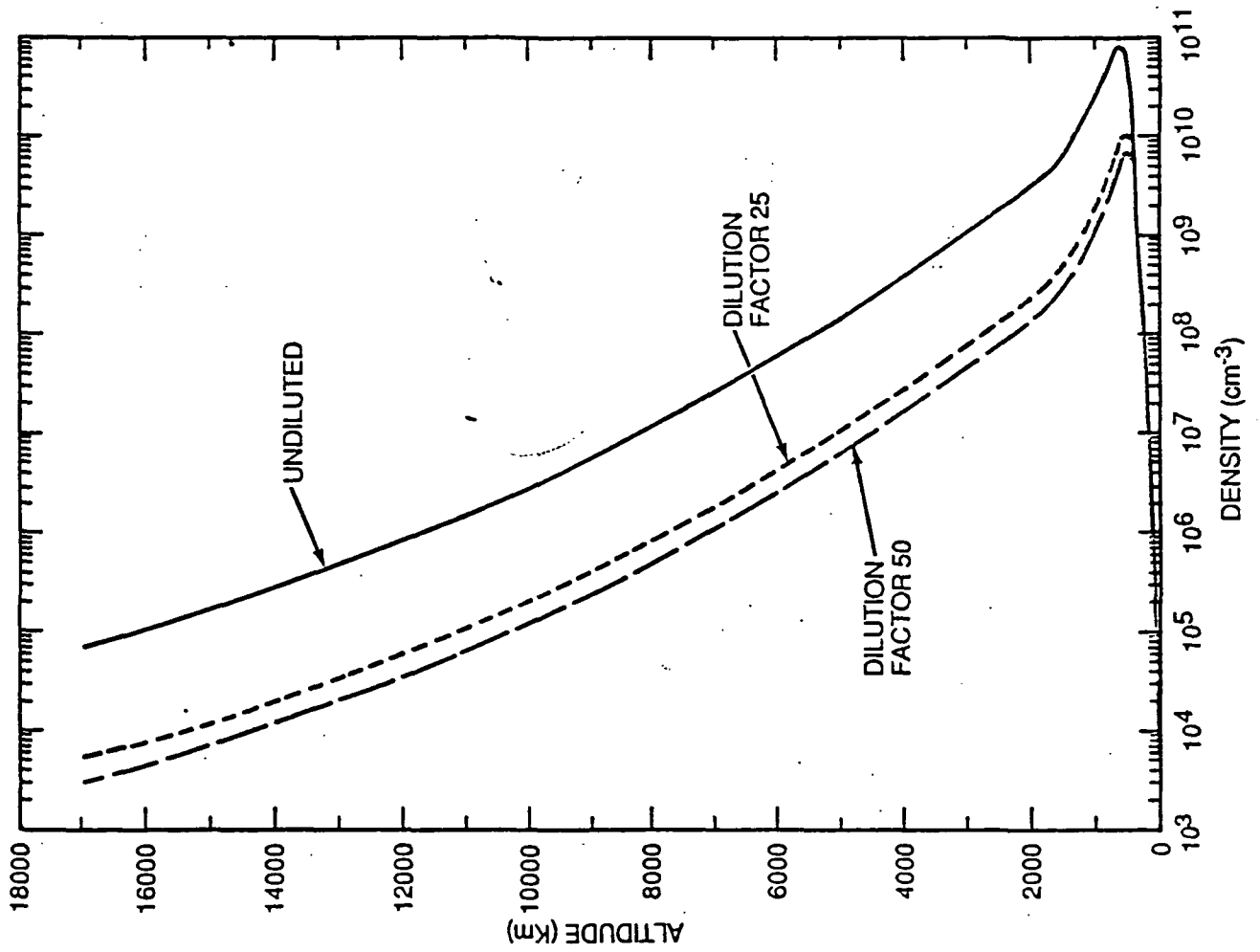


Figure 8a

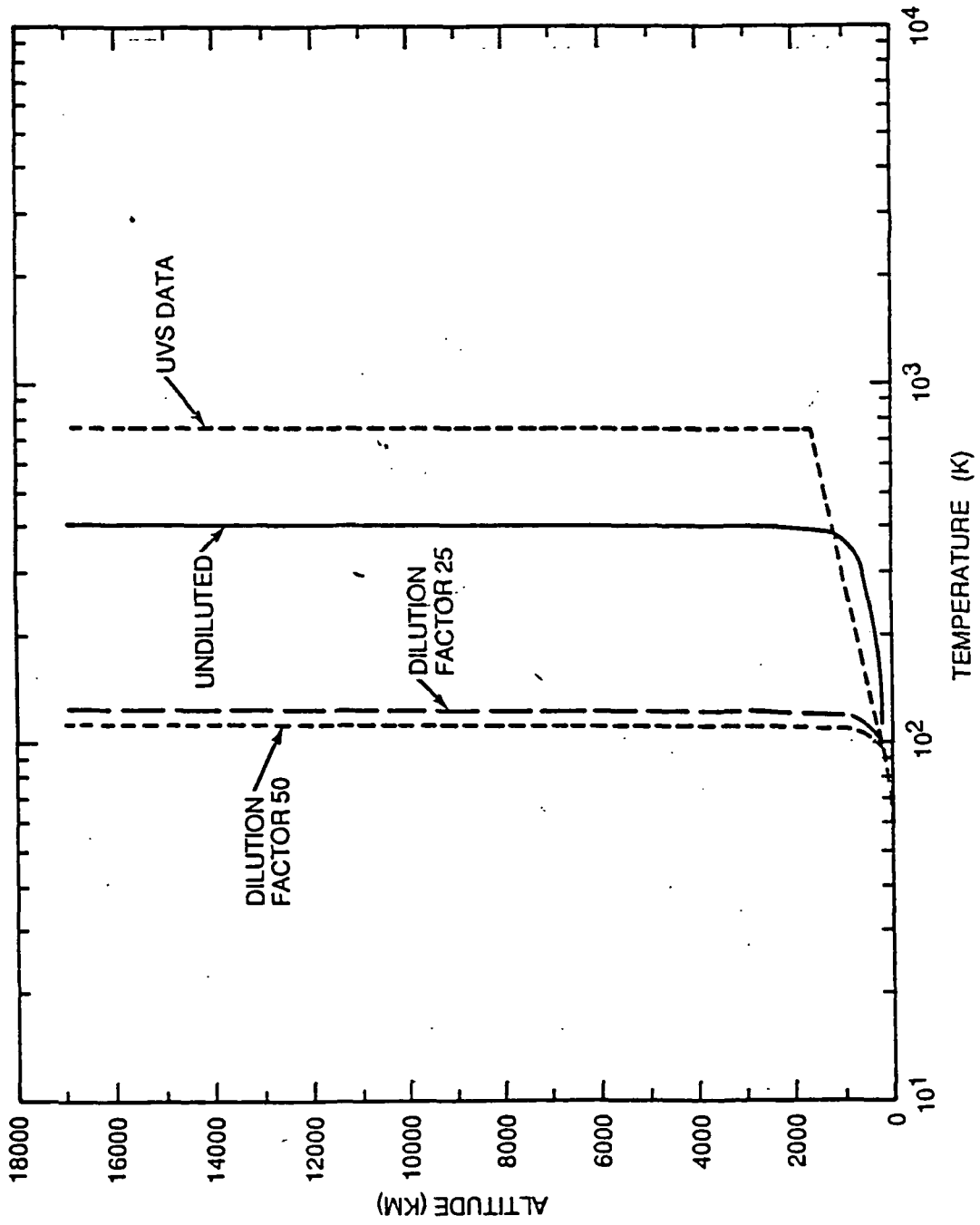


Figure 8b

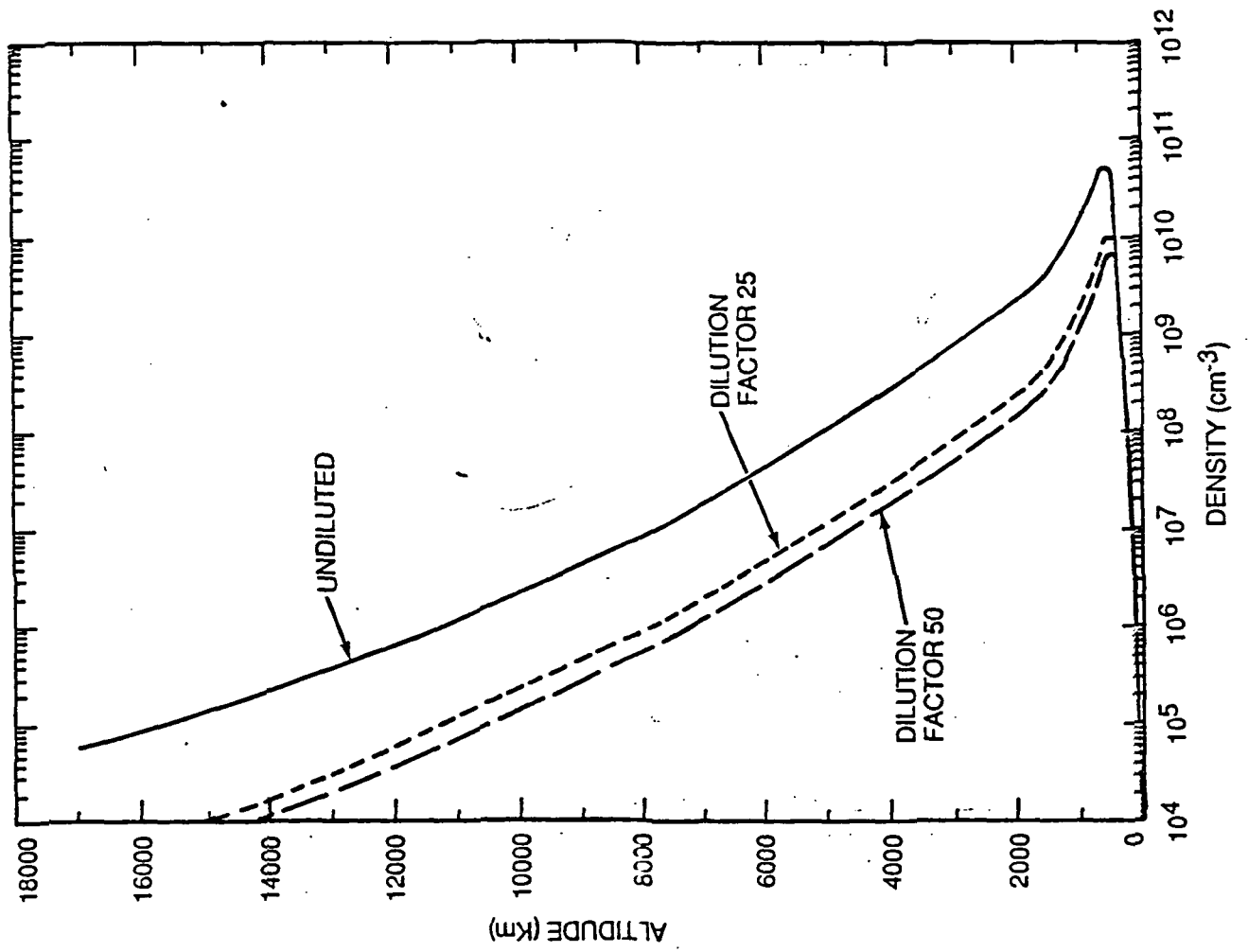


Figure 9a

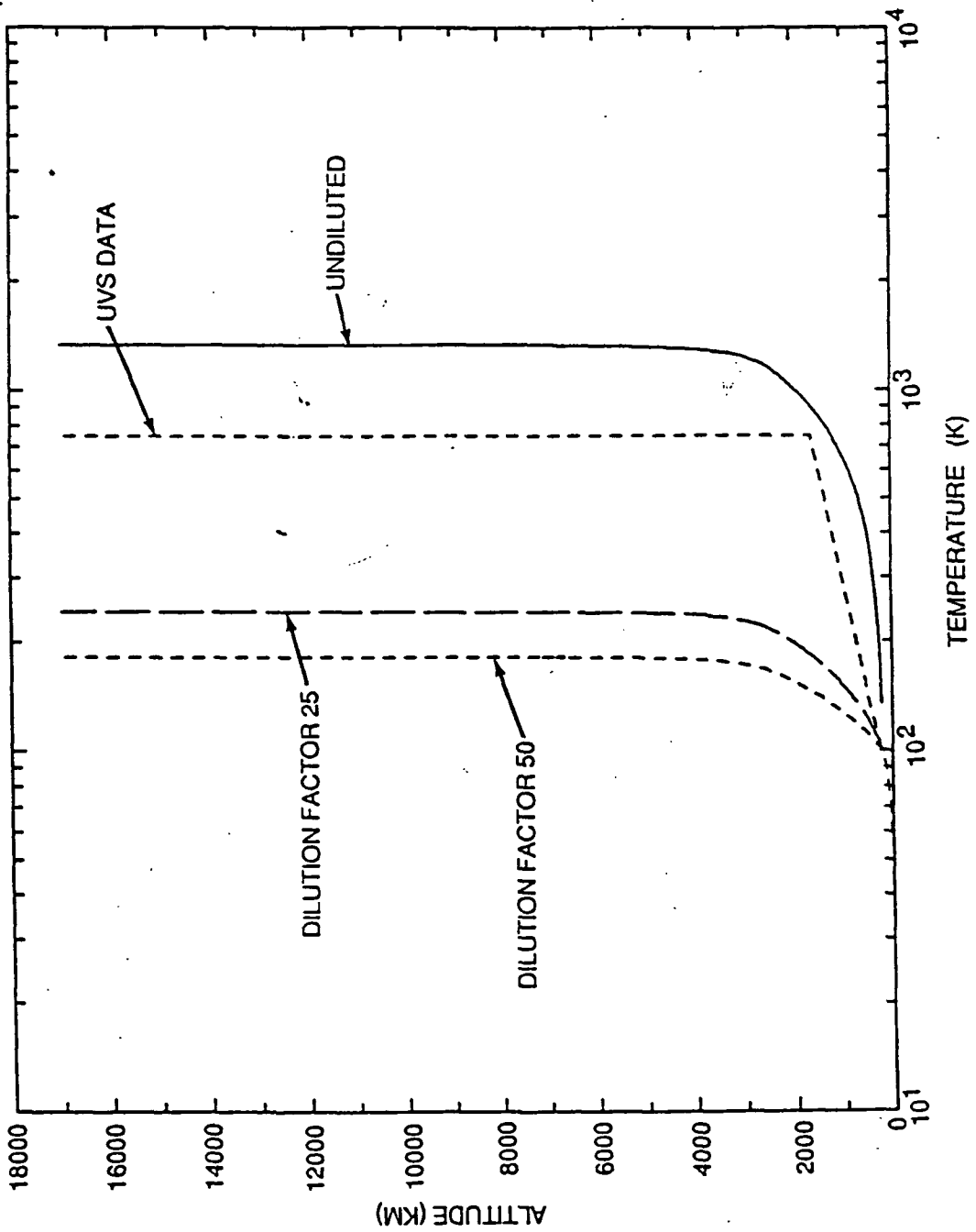


Figure 9b